THERMAL STRAIN EFFECTS IN THERMOPLASTIC SATIN WEAVE COMPOSITE LAMINATES

E. Voet[a*], G. Luyckx[a], W. Van Paepegem[a] , J. Degrieck[a]

[a] *Ghent University, Department Mechanics of Materials and Structures, Technologiepark-Zwijnaarde 903, 9052 Zwijnaarde (Belgium)*

**eli.voet@ugent.be*

Keywords: thermoplastic composite, embedded FBG, annealing, residual strain.

Abstract

In this research, thermoplastic carbon-PPS woven fabrics are subjected to temperature cycles from -20 °C till 160 °C. All samples have embedded fibre Bragg gratings in the symmetry-plane of the laminates. It will be shown that heating above the T_g reverses more or less the thermal residual strains and that after cool-down the spectral response of the fibre Bragg gratings has changed, proving the annealing effect. Although macroscopically the two different lay-ups are identical, the results show that thermal strain in the symmetry plane is significantly influenced by the composite's stacking sequence.

1 Introduction

If composite laminates are subjected to temperatures above their glass-transition temperature (Tg), relaxation or crystallisation takes place which is, in analogy to isotropic materials, referred to as an annealing effect [1]. Composite annealing is often carried out on thermoplastic fibre reinforced plastics to relax residual stresses, to minimize the residual strain gradient through the thickness or to obtain optimal levels of crystallinity [2, 3, 4]. Moreover, by performing an annealing cycle, the stress-free temperature of a composite may effectively be altered [2].

In this research, four thermoplastic (PPS) CFRP laminates with embedded Fibre Bragg Gratings (FBGs) are put in a climate chamber and subjected to temperatures from -20 °C till 160 °C. The maximum temperature during cycling is exceeding the T_g (90 °C) of the PPS-matrix, hence annealing effects take place in the composite laminates.

The embedded FBGs are used to characterize the thermal behaviour of the CFRP laminates. Specifically the use of the spectral response is elaborated during temperature cycling to investigate in-situ temperature effects during heating and cooling, moreover all readings are compared before and after cycling. As such it is possible to determine the release of residual strains.

2 Materials and methods

2.1 Thermoplastic composite laminates

The material studied is an advanced carbon fibre reinforced thermoplastic, called CETEX®, provided by TenCate (The Netherlands). It has a PPS (PolyPhenylene Sulfide) matrix reinforced with a 5-harness satin weaving pattern with T300JB carbon fibres and 3000 filaments per yarn. The laminates are stacked using carbon-PPS woven fabrics, or semi-pregs, notation (0,90), with the 0 degrees corresponding to the warp direction of the weave (Figure 1). The carbon PPS plates are manufactured using a hot press technique. Test-coupons were cut from the large laminate using a water-cooled diamond saw with dimensions according to the ASTM D3479 tension-tension fatigue standard (300mm x 28mm x 2.4mm), in function of mechanical tests after thermal testing.

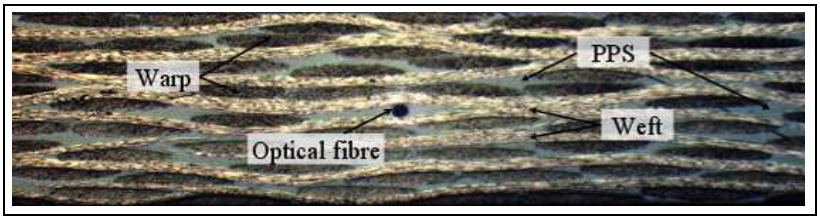

Figure 1: Cross-section of a $[(0,90)]_{4S}$ stacked Cetex® laminate with warp and weft yarn interlacing pattern and embedded optical fibre in the centre.

2.2 Embedded fibre optic sensors in different laminate lay-ups

All samples have embedded fibre Bragg gratings in the centre of the symmetry-plane of the laminates. The optical fibres are always oriented parallel to the warp direction. Two specimens with stacking sequence $[(0,90)]_{4S}$ and two with stacking sequence $[(90,0)]_{4S}$ are prepared. Both lay-ups have the warp (0°) and weft (90°) yarns in the same direction, hence macroscopically the properties are found the same. However their symmetry-plane (=plane of embedding) is different as shown in Figure 2, where we see an example of the cross-section and symmetry-planes of both lay-ups with in the centre the embedded optical fibres.

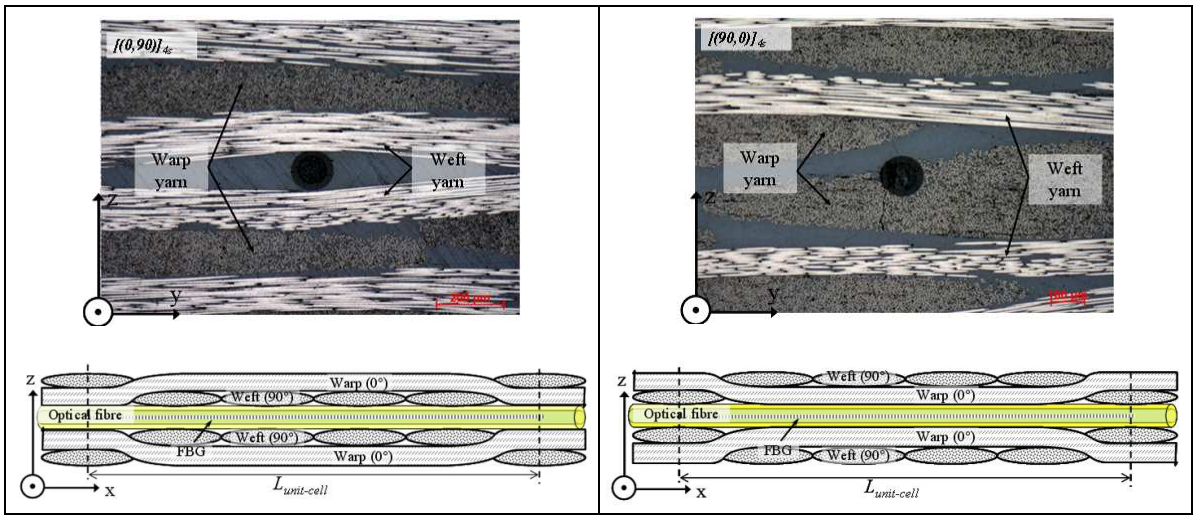

Figure 2: Optical fibre embedded in a symmetrical stacked woven fabric laminate: $[(0,90)]_{4S}$ type stacking (left), and $[(90,0)]_{4S}$ type stacking (right)

The optical fibres have a cladding diameter of 125µm and an outer diameter of 190µm with ORMOCER coating [5]. Each sample has one optical fibre with one FBG in the centre.

2.3 Determination of the transverse strain difference

In this research, we use the optical birefringence of the embedded FBGs to estimate the residual transversal strain difference for the woven fabrics. Due to the severe distortion of the spectrum, the author uses controlled (linear) polarization testing to better analyse the individual FBG spectra with regard to the induced birefringence. The spectrum at each polarization angle is recorded, and by using the well-known centre of gravity (COG) algorithm, the centroid wavelength is determined. An example of the development of the COG wavelength against the linear polarization angle for one FBG, is shown in Figure 3, left. We can clearly see the sinusoidal shape with a maximum wavelength at 40° (peak2) and a minimum wavelength (peak1) at 130°. The corresponding minimum and maximum distorted Bragg peaks are shown in Figure 3, right. The wavelength difference between the centroid wavelengths of both peaks is a measure for the mean birefringence effect which is present in the core of the FBG.

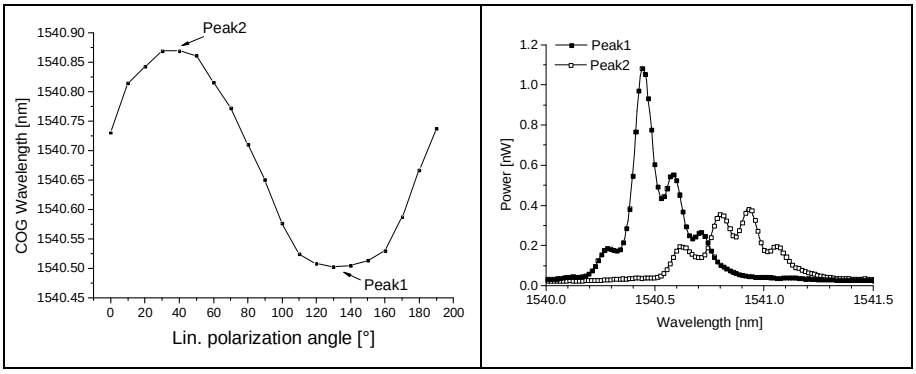

Figure 3: Development of the centroid wavelength against the linear polarization angle (Left), Polarized spectra according 1' and 2' axis (right)

From the maximal peak separation the transverse strain difference in the optical fibre is then determined by [6]:

$$\varepsilon_{1'} - \varepsilon_{2'} = \Delta\varepsilon_{trans} = \frac{2}{\bar{n}^2} \frac{\lambda_{B,1'} - \lambda_{B,2'}}{\left(\lambda_{B,0}\right)\left(p_{12} - p_{11}\right)} . \quad (1)$$

With p_{11} and p_{12} the strain-optic coefficients, $\bar{n}$ the effective refractive index of the optical fibre, $\lambda_{B,1'}$ the minimal, and $\lambda_{B,2'}$ the maximal COG wavelengths (as depicted in Figure 3) and $\lambda_{B,0} = \frac{\lambda_{B,1'} + \lambda_{B,2'}}{2}$ the mean COG wavelength, at each temperature level, we can determine from Equation (1) the evolution of the transverse strain state during temperature cycling.

3 Experiments and results

3.1 Measurement setup

To investigate the annealing effects, two specimens of each lay-up (i.e. $[(0,90)]_{4S}$ and $[(0,90)]_{4S}$) are put in a climate chamber (Figure 4) with the FBGs of all four samples connected to a commercial FOS&S FBG-scan X08 interrogator to analyse their spectral response during temperature cycling. The temperature readings of a Pt100-probe which is put

next to the plates and the measurements with the FBG-scan are synchronized using a Labview based software program.

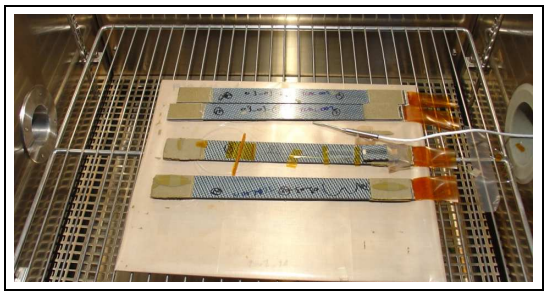

Figure 4: Test-coupons placed in a climate chamber to perform temperature tests. A Pt-100 probe is placed next to the samples to register the temperature.

3.2 Thermal cycling

All four samples, as shown in Figure 4, are subjected to the same temperature cycles to investigate composite annealing and possible differences in thermal response for the two lay-ups.

Two approaches are used:
First a temperature cycle (Cycle I) is executed in two steps using the following temperature sequences:

- 20 °C (initial measurement 'before'),
- Cycle Ia: from -20 °C till 60 °C (Figure 5, right),
- Cycle Ib: from 40 °C till 160 °C (Figure 5, right).

At each temperature level the Bragg spectrum of all samples is recorded and a full polarization sweep (0° – 190°) is performed (as explained in Section 2.3) to analyse the birefringence effects and to calculate the transverse residual strain release.

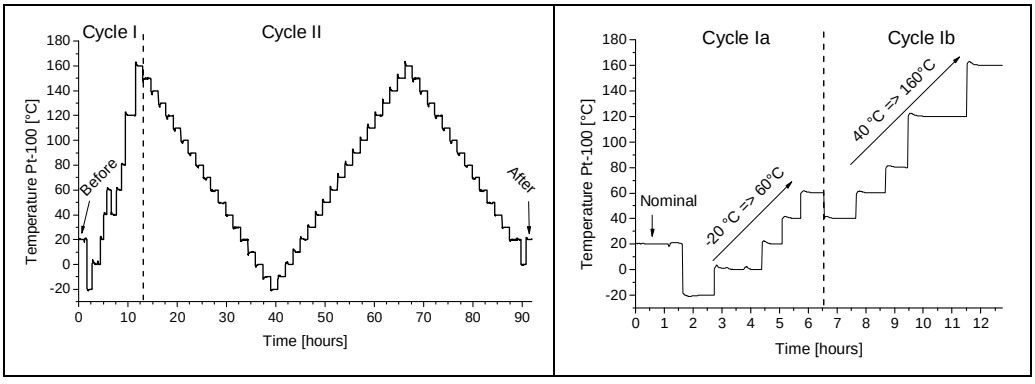

Figure 5: Complete temperature profiles from -20 °C till 160 °C divided in two cycles (left), detail of Cycle 1 (right)

After the first temperature cycle the COG wavelength of the full de-polarized spectra of all FBGs is followed during a second temperature cycle (Cycle II) which is executed in three steps:

- Cycle IIa: 160 °C till -20°C
- Cycle IIb: -20 °C till 160 °C
- Cycle IIc: 160 °C till 0°
- 20°C (measurement 'after')

Cycle II is used to compare (i.e. characterize) the macroscopic thermal behaviour of both types of laminates by analysing the global peak shift as function of temperature. The Bragg peak response will be further discussed in the next Section.

3.3 Total Bragg peak response

To illustrate the influence of the thermal strains in the composite at different temperatures, the Bragg response from room temperature up to 160 °C is shown in Figure 6 for a $[(0,90)]_{4S}$ laminate (sample n°7) and for a $[(90,0)]_{4S}$ laminate (sample n°11). We observe from the spectra that the 'initial' distortion at 20 °C of the Bragg peak in the $[(0,90)]_{4S}$ sample is more heavy and wider than the Bragg peak in the $[(90,0)]_{4S}$ sample, which indicates that the residual strain state in the symmetry-plane is clearly different.

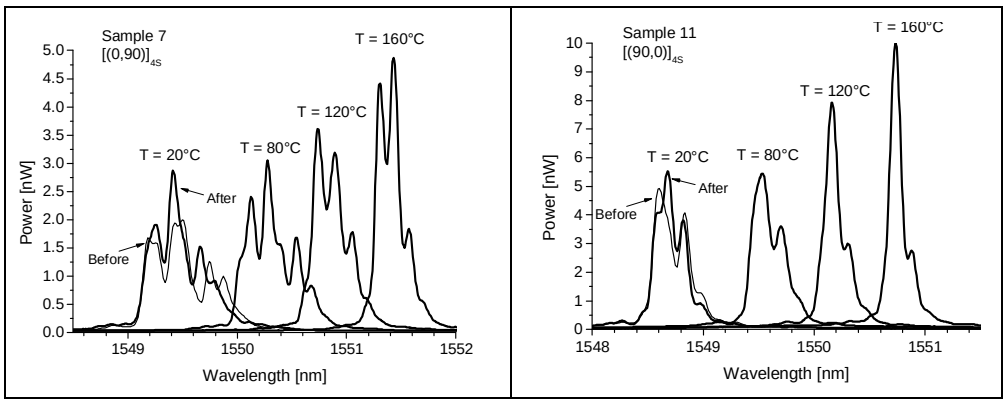

Figure 6: Spectral response for sample n°7 ($[(0,90)]_{4S}$) (left), and sample n°11 ($[(90,0)]_{4S}$) (right) at different temperatures. The spectrum at 20°C before and after the test is indicated in each graph.

However for both samples, we notice that the peak distortion decreases when temperature is increased, and as a consequence the width of the spectra is reduced. Moreover, for sample n°11 we even see that the Bragg peak at 160 °C becomes almost non-distorted. This illustrates that the effect of heating reverses the thermal induced strains in the composite. Obviously, the transverse strain difference changes as well. A permanent change of the spectra at 20 °C is observed as well; if we compare the spectrum recorded at 20 °C before and after the temperature cycling, the Bragg spectra of both samples changed indicating a residual strain release. This effect is further explored in the following subsection.

3.4 Transverse residual strain release

To study the birefringence in the embedded FBGs during thermal testing the procedure of polarization testing is applied (see Section 2.3) . An example of the spectral response of the 'fast' and 'slow' peak of the embedded FBG in sample n° 7 at the two extreme temperatures (-20 °C and 160 °C) is shown in Figure 7, left, with the de-polarized spectra plotted as well (dashed lines). As expected from the narrowing of the peaks seen in Figure 6, the transverse strain difference in the $[(0,90)]_{4S}$ is high at lower temperatures and it decreases at higher

temperatures. The evolution of the calculated transverse strain difference from Equation (1) against temperature for all samples during Cycle I, is shown in Figure 7, right.

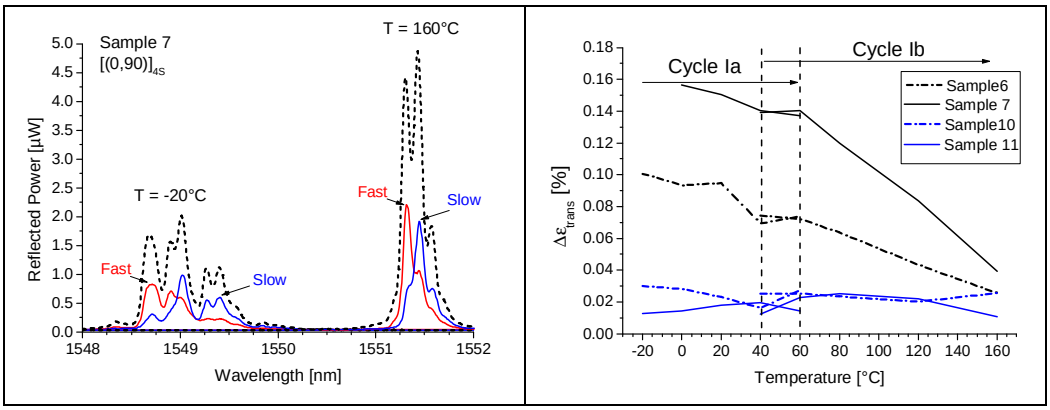

Figure 7: Spectral response of the 'fast' and 'slow' peak for sample n°7 at -20 °C and 160 °C (left), evolution of the transverse strain difference $\Delta\varepsilon_{trans}$, against temperature for all samples during Cycle Ia and Cycle Ib (right).

Although the transverse strain difference changes clearly for the $[(0,90)]_{4S}$ samples, the effect is not manifesting in the $[(90,0)]_{4S}$ samples; only a very small decrease is found for sample n°10, and no clear course is found in the strain evolution of sample n°11. As such we can conclude that the transverse thermal strains in the mid-plane layers of the $[(90,0)]_{4S}$ lay-up are much lower compared to the $[(0,90)]_{4S}$ lay-up, which confirms that the residual transverse strain formation in the mid-planes of the $[(90,0)]_{4S}$ laminate during consolidation is much lower too.

To investigate the annealing effect or residual strain release, similar to the spectra 'before' and 'after' shown in Figure 6, the author compares the transverse strain difference of all samples measured at 20 °C before and after the complete temperature test. The de-polarized spectra of all four samples before and after the test are shown in Figure 8.

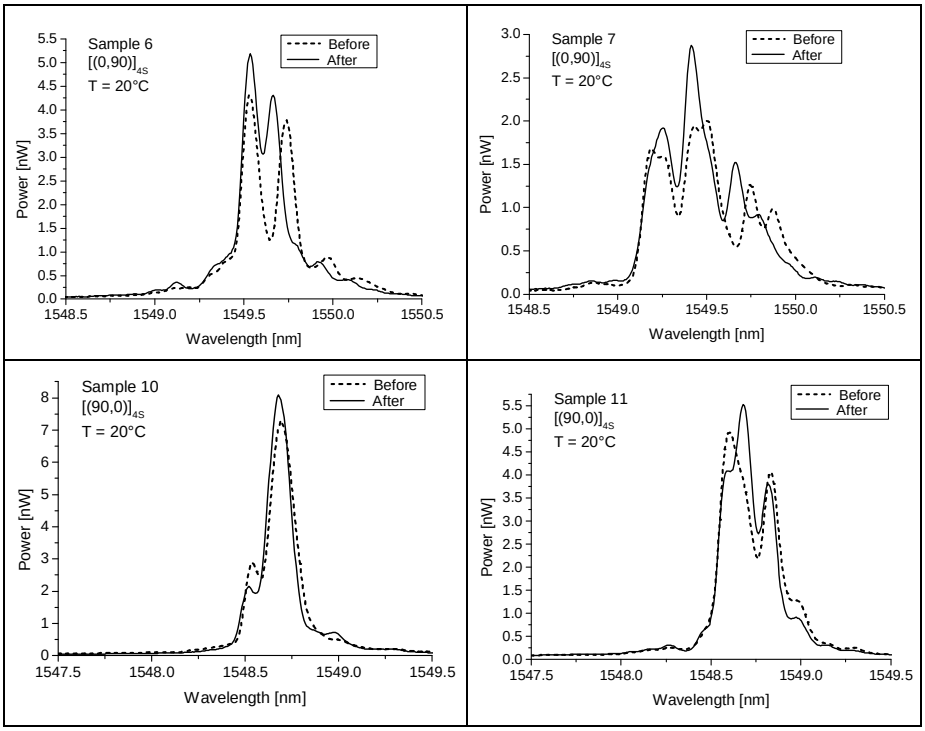

Figure 8: Spectral response (de-polarized) at 20 °C, before and after the temperature test, for all samples.

We observe that all Bragg spectra have changed shape, however, the effect is most significant in the $[(0,90)]_{4S}$ stacked laminates. The individual peaks are shifted and the peak width after the test is narrower, which proves that the strain state around the optical fibre has changed.

The transverse strain difference is calculated from the change in birefringence effects for all samples using Equation (1), the values are given in Table 1.

		$\Delta\varepsilon_{trans}$ [%]	
n°		Before	After
6	$[(0,90)]_{4S}$	0.0812	0.0283
7	$[(0,90)]_{4S}$	0.1450	0.1099
10	$[(90,0)]_{4S}$	0.0233	0.0173
11	$[(90,0)]_{4S}$	0.0212	0.0241

Table 1: Transverse strain for all samples, $\Delta\varepsilon_{trans}$ at 20°C, before and after the temperature test.

As expected, no significant transverse residual strain release is found in case of the $[(90,0)]_{4S}$ lay-up, however, in case of the $[(0,90)]_{4S}$ stacked laminates, the value of $\Delta\varepsilon_{trans}$ for sample n°6 and sample n°7 has decreased with approximately 300 % and 30 %, respectively. We notice that the distribution of the results is large which proves that the local residual strain in the woven fabric composite is complex and varies significantly along the length of the unit cell.

4 Conclusions

Two types of lay-up of the carbon-PPS woven fabric are investigated by using embedded FBGs. It is shown that the material exhibits a complex local strain distribution because of its weave pattern, causing the Bragg spectra of the embedded FBGs to be heavily distorted. This effect is seen immediately after manufacturing, and is more distinct in the mid-plane layers of the $[0,90)]_{4S}$ lay-up.

Results from the spectral response during heating reverses more or less the thermal residual strains. The shape of the spectrum at 160 °C is close to the undistorted spectral shape. If the material is cooled down again, the spectral shape has changed compared to the initial spectrum before heating. This proves that annealing effects take place. The measured transverse strain difference in the FBGs decreases significantly in case of the $[(0,90)]_{4S}$ stacked laminates (~300 %), however, no significant effects are noticed for the samples with $[(90,0)]_{4S}$ lay-up. Although macroscopically the two different lay-ups are identical, the results show that the thermal strain in the symmetry plane is significantly influenced by the stacking sequence.

Even though the Cetex® material has a complex (thermal) material behaviour, the results in this paper have certainly shown that the embedded FBG is a valuable tool to study the internal thermal strain states in thermoplastic (woven-fabric) fibre reinforced plastics.

5 Acknowledgements

The authors would like to thank TenCate Advanced Composites (the Netherlands) for the supply of the CETEX® material, FBGS-technologies and IPHT-Jena (Germany) for their support during new fibre developments and FOS&S for the loan of their equipment.

References

[1] Barnes, J.A., *Thermal-expansion behavior of thermoplastic composites.2.* Journal of Materials Science, 1993. **28**(18): p. 4974-4982.
[2] Barnes, J.A. and Byerly, G.E., *The formation of residual-stresses in laminated thermoplastic composites.* Composites Science and Technology, 1994. **51**(4): p. 479-494.
[3] Manson, J.A.E. and Seferis, J.C., *Process simulated laminate (PSL)- a methodology to internal-stress characterization in advanced composite materials.* Journal of Composite Materials, 1992. **26**(3): p. 405-431.
[4] Unger, W.J. and Hansen, J.S., *The effect of cooling rate and annealing on residual-stress development in graphite fiber reinforced PEEK laminates.* Journal of Composite Materials, 1993. **27**(2): p. 108-137.
[5] FBGS-technologies GmbH, available from http://www.fbgs.com .
[6] Bosia F et al., "Characterization of the response of fibre Bragg grating sensors subjected to a two-dimensional strain field", Smart Mater. Struct., 2003. 12, 925–34